NASA TECHNICAL MEMORANDUM

NASA TM X-52975

NASA TM X-52975

THERMAL-FATIGUE RESISTANCE OF 15 HIGH-TEMPERATURE ALLOYS DETERMINED BY THE FLUIDIZED-BED TECHNIQUE

by David A. Spera
Lewis Research Center
Cleveland, Ohio

Maurice A. H. Howes
IIT Research Institute
Chicago, Illinois

and

Peter T. Bizon
Lewis Research Center
Cleveland, Ohio

TECHNICAL PAPER proposed for presentation at
Western Metal and Tool Exposition, Conference, Design and Scientific Precision Instruments Exhibit (WESTEC) sponsored by the
American Society for Metals
Los Angeles, California, March 8-11, 1971

ABSTRACT

Thermal-fatigue tests were conducted on B 1900, IN 100, IN 100 DS (directionally solidified), MM 200, MM 200 DS, IN 162, IN 713C, M 22, TAZ 8A, U 700 (wrought and cast), TD NiCr, X 40, WI 52, and MM 302. Alloys B 1900, IN 100, and IN 100 DS were also tested with aluminide coating. Among the 18 materials tested, cycles to cracking differed by more than two orders of magnitude. Coating and directional solidification were of definite benefit. However, the directionally solidified alloys suffered considerable weight loss through oxidation. Cycles to cracking were calculated theoretically for IN 100 and B 1900, coated and uncoated, and were in agreement with the data.

E-6182

THERMAL-FATIGUE RESISTANCE OF 15 HIGH-TEMPERATURE ALLOYS DETERMINED BY THE FLUIDIZED-BED TECHNIQUE

David A. Spera
National Aeronautics and Space Administration
Lewis Research Center
Cleveland, Ohio

Maurice A. H. Howes
IIT Research Institute
Chicago, Illinois

and

Peter T. Bizon
National Aeronautics and Space Administration
Lewis Research Center
Cleveland, Ohio

SUMMARY

This investigation is part of a general study of thermal fatigue conducted at the NASA-Lewis Research Center. This program used the fluidized-bed heating and cooling technique to measure the relative thermal-fatigue resistance of 15 nickel- and cobalt-base alloys. These alloys were B 1900, IN 100, IN 100 DS (directionally solidified), MM 200, MM 200 DS, IN 162, IN 713C, M 22, TAZ 8A, U 700 cast, U 700 wrought, TD NiCr, X 40, WI 52, and MM 302. Three alloys--B 1900, IN 100, and IN 100 DS--were also tested with an aluminide coating. Tests were performed at IIT Research Institute under contract to NASA. Resistance to thermal fatigue was measured by cycling groups of specimens between fluidized-beds operating at 1360 K (1990 F) and 590 K (600 F). Cycle times varied from four to eight minutes and equal periods of time were spent in heating and cooling. The number of cycles required to generate the first crack was used as the measure of the thermal-fatigue resistance of the material. Crack propagation data were also taken.

The most crack-resistant materials were those which were either coated or directionally solidified, or both: MM 200 DS, IN 100 DS,

IN 100 DS (coated), and B 1900 (coated). Among the 13 uncoated conventionally cast and wrought alloys, TAZ 8A and X 40 had the highest thermal-fatigue resistance.

Directional solidification of MM 200 increased its relative resistance to thermal fatigue by a factor of at least several hundred, from the lowest to the highest of the alloys tested. This indicates the importance of grain structure to thermal-fatigue resistance, as compared to composition. However, oxidation rates were much higher in the uncoated directionally-solidified alloys than in any of the conventionally cast materials.

Cracks in alloys with low thermal-fatigue resistance tended to be intergranular. Alloys with high resistance tended to exhibit transgranular cracks.

Thermal fatigue theory was used to calculate cycles to cracking for two alloys: IN 100 and B 1900, both coated and uncoated. This theory considers both low-cycle fatigue and cyclic creep failure. In general, calculated and observed lives were in good agreement, verifying the stress analysis and thermal fatigue theory for conventionally cast alloys.

INTRODUCTION

The objective of this investigation was to measure the resistance to thermal fatigue of 15 alloys. These alloys might be used in the hottest sections of aircraft gas turbines. The primary purpose for obtaining these data was to verify a theory for predicting thermal fatigue life (Ref. 1). Results are therefore presented in two parts: (1) tables and graphs of cycles required for cracking of the 15 alloys, with representative photographs and micrographs; and (2) comparison between theoretical and observed cycles to cracking for two of the alloys, each in the coated and uncoated conditions. These are the only two alloys for which calculations have been made to date.

This investigation is one part of a general study of thermal fatigue conducted at the NASA-Lewis Research Center. Other parts of the

study are shown schematically in Fig. 1 and described in Ref. 2.

Thermal fatigue is a potential mode of failure in any heat engine or piece of high-temperature machinery. Thermal fatigue is defined as the cracking of a material primarily by alternate heating and cooling. Such heating and cooling is almost always nonuniform. This results in cyclic thermal stress which in turn causes thermal-fatigue cracking. Modern gas turbines are particularly susceptible to thermal fatigue. They are operating at higher and higher temperatures in the search for increased efficiency, thrust, and economy. Service times are also being lengthened. These are just the circumstances which can make thermal fatigue a dominant mode of failure.

Thermal fatigue resistance is becoming one of the most important qualities to be considered when selecting an alloy for a high-temperature part. Unfortunately, it is not an easily measured material property like tensile strength, ductility, or creep-rupture strength.

Strictly speaking, thermal-fatigue resistance is not a basic material property, but a structural response. It is a complex combination of geometry, loads, temperatures, ductility, oxidation resistance, and many other factors. Therefore, in this study, the term "thermal-fatigue resistance" is used in a relative, rather than absolute, sense. Alloys are compared to one another, all having been tested under identical conditions.

The absolute number of cycles to cracking is too dependent on test conditions and specimen geometry to be of general use. Test conditions in this study were selected to represent advanced gas turbine engines. In this respect they were usually more severe than present use conditions. For example, a maximum bed temperature of 1360 K (1900 F) was used for all tests. This is well above the present use temperature of many of the alloys tested.

Fluidized beds were first used for comparative thermal-fatigue testing in 1958 by Glenny and his co-workers at the National Gas Turbine Establishment in England (Ref. 3). Since that time the technique has become widely accepted for evaluating the thermal-fatigue behavior of

both alloys and components. Refs. 4 to 7 describe some of this work.

The work described herein was carried out in a facility designed, built, and operated by the IIT Research Institute, under contract to NASA. Details of the test procedure and the raw data from the investigation are given in Ref. 8.

EXPERIMENTAL PROCEDURE

Relative thermal-fatigue resistance was determined experimentally by testing different alloys simultaneously and comparing the cycles required to produce the first crack. Groups of wedge-shaped specimens were alternately heated and cooled rapidly in beds of fluidized particles. The heating bed was held at 1360 K (1990 F) while the cooling bed temperature was 590 K (600 F). Five different cycle times and six specimens of each material were used: two specimens at four minute cycles, and one specimen each at five, six, seven, and eight minute cycles. Cycle times were divided equally between heating and cooling.

Crack data were obtained using the following procedure: Periodically, specimens were removed from the test fixture, and both edges were examined for cracks using a 30X traveling microscope. Only the surfaces within ±2.5 centimeter of mid-length were examined. When a crack was discovered in this region, its length on each side and its location were measured. The crack area was then calculated assuming the crack front to be a straight line. Crack initiation and propagation were determined in this way for the first three cracks in each edge.

Alloys and Specimens

Fifteen alloys were studied in this program. These are listed in Table I together with their compositions. Three alloys were given an aluminide coating, bringing to eighteen the number of different materials tested. Table II lists the various heat-treatments applied to the alloys.

Two types of specimens were produced, as shown in Fig. 2. These

are a double-wedge shaped bar for thermal-fatigue testing and a round bar for measuring tensile and creep-rupture properties. Sample mechanical properties are listed in Tables III and IV for fourteen of the alloys.

Specimens were cast-to-size from the eleven conventionally cast alloys. Inoculated molds were used to produce fine grain structures. The directionally solidified specimens were cast oversize and machined to final dimensions.

Fluidized-Bed Facility

The fluidized-bed thermal-fatigue facility is shown schematically in Fig. 3. The facility is described in detail in Ref. 8. As shown in the figure, the beds are used in pairs--one each for heating and cooling. A bed consists of a retort filled with fine sand through which air is pumped. The flow of air causes the sand particles to develop a churning, circulating action. In this way the bed is "fluidized". The large mass of the beds and their circulatory motion promote uniform, high heat-transfer rates.

The facility used in this investigation consisted of a 30 centimeter (12 in.) diameter heating bed situated between two 36 centimeter (14 in.) diameter cooling beds. The heating bed contained 1100 N (250 lb) of 28-to 48-mesh tabular alumina. Power input was 55 kilowatt and air flow was 17 m^3/hr (600 ft^3/hr). Each intermediate bed contained 1500 N (340 lb) of alumina, used 12 kilowatts of power and had an air flow of 60 m^3/hr (2100 ft^3/hr). As many as 18 specimens were tested simultaneously, using the holder shown in Fig. 4.

Transient Temperature Measurements

Transient temperatures were measured in five alloys, using imbedded thermocouples. Fig. 2(a) shows the five points at which thermocouples were placed. The alloys calibrated were IN 100, wrought U 700, MM 200, MM 302, and WI 52. Data were taken for

cycle times of four, six, and eight minutes. These data can be used to compute transient thermal stresses for all alloys in this program as they represent a range of thermal conductivities. For example, in this study, B 1900 temperatures were assumed to be given by the MM 200 temperature data. These two alloys have approximately the same conductivities and diffusivities.

EXPERIMENTAL RESULTS

Cycles to First Crack

Table V summarizes the crack initiation data obtained in this investigation. The number of cycles to the first crack is assumed to be halfway between the last inspection cycle without cracks and the first inspection cycle with cracks. These data include only those cracks within the center five centimeters of the specimen length.

The benefits of directional solidification and coating are obvious. Directional solidification raised the thermal-fatigue resistance of MM 200 from the lowest of the 18 materials tested to the highest. As another example, IN 100 cracked in 38 six-minute cycles, while coated IN 100 lasted 400 cycles, and directionally solidified IN 100 endured 4200 thermal cycles before cracking. However, coating of IN 100 DS reduced its thermal-fatigue resistance somewhat. Apparently a change in the grain structure of an alloy can change the effectiveness of a coating in preventing cracks. Fig. 5 shows the thermal-fatigue resistance for the six-minute cycle tests in graphical form.

The relative resistance to cracking of all the alloys can be given numerically if one alloy is used as a standard of comparison. For convenience, TAZ 8A was selected as the standard for this investigation. It had the highest thermal-fatigue resistance among the alloys for which all six specimens cracked. The last two columns in Table V and the bar chart in Fig. 6 give relative resistance as a percent of the resistance of TAZ 8A. This is given for both the six-minute cycle (in which all materials cracked) and for all the cycles. The results are very

similar for both cases. The results in Fig. 6 were used to check several empirical formulas for predicting relative thermal-fatigue resistance. These formulas generally use tensile or creep-rupture test data. For example, a simple formula is proposed in Ref. 5 which uses yield strength and tensile elongation. No correlation was found between predicted and observed thermal-fatigue resistance using any of the empirical formulas that were checked.

Oxidation

The 15 alloys exhibited a wide variation in oxidation resistance (ref. 8). This is shown in Fig. 7, which is a series of photographs of tested specimens. In general, the alloys with the highest oxidation resistance had the highest thermal-fatigue resistance. The directionally solidified alloys were an exception to this rule. They oxidized faster than any of the conventional alloys yet had the highest thermal fatigue resistance. Weight losses as high as 3-6 percent per 1000 cycles were measured during the 8-minute cycle tests. The original edge radii were greatly reduced, producing sharp edges. Normally this would increase thermal stresses and accelerate cracking. However this was not the case with the columnar grained materials.

As shown in Fig. 7, coated IN 100 DS exhibited swelling rather than erosion. This indicated that oxidation took place under the coating. However, weight loss was at a much lower rate than in the uncoated alloy. The swelling is further evidence that the coating was not optimized for the directional form of IN 100. Optimizing a coating for a directionally-solidified alloy is inherently difficult. The coating re-introduces the transverse grain boundaries which were eliminated by growing columnar grains in the substrate. A compromise between thermal-fatigue resistance and oxidation resistance may be necessary in directionally solidified alloys.

Crack Propagation

Both transgranular and intergranular cracks were observed in this investigation. As a rule, transgranular cracks were typical of alloys with high resistance to thermal fatigue. Alloys with very low resistance almost always had intergranular cracks. Apparently a prerequisite for increasing thermal-fatigue resistance is the suppression of intergranular cracking. This can be done by compositional changes, coatings, or directional solidification.

Fig. 8(a) shows typical transgranular cracks in TAZ 8A and IN 100 DS. Straight paths perpendicular to the surface are characteristic of transgranular cracks. In TAZ 8A the straight edge of the specimen and the uniform width of the crack indicate it did not start at an oxidation pit. These micrographs suggest that intergranular cracks can be suppressed by (a) a heavily laced dendrite structure as in TAZ 8A, as well as (b) by the absence of transverse grain boundaries, as in IN 100 DS.

Fig. 8(b) shows typical intergranular cracks in alloys with low thermal-fatigue resistance. The cracks start at surface oxidation pits and proceed in zig-zag patterns between grains. Early failure at grain boundaries prevents these alloys from using the available strength within the grains themselves.

Examination of Fig. 7 reveals several additional points about crack propagation: First, cracks can propagate to considerable lengths under the action of thermal stress alone. In alloys with conventional structure, cracks stopped growing only when they reached the thicker, low-stress regions of the specimens. On the other hand, a columnar-grained structure arrested cracks at very short lengths.

Second, multiple cracks generally occurred at uniform intervals along the specimen edges. Apparently a crack relieves stresses in its immediate neighborhood, preventing growth from nearby crack nuclei.

Third, longitudinal cracks often nucleated at the locating grooves on the ends of the specimens. This was particularly important in alloys with transverse strength much lower than longitudinal strength.

TD NiCr, for example, exhibited very large longitudinal cracks which started at the locating grooves. These are clearly seen in Fig. 7. Also shown in the figure is a transverse crack in TD NiCr which has started to turn and propagate longitudinally. Thus, stress concentrations in nominally low-stress regions may cause unexpected cracks, particularly in anisotropic materials.

Fig. 9 shows crack growth rates for coated and uncoated IN 100 and B 1900. These data are for the largest crack in the first edge of the specimen to fail. As shown in the figure, crack growth can be correlated with cyclic life in the uncoated condition.

As might be expected, coating of IN 100 and B 1900 did not change the rate of crack growth. The propagation rate was inversely proportional to the number of cycles required to start the crack. This rate is approximately constant for crack areas less than the quantity, C, the curve-fit constant defined in Fig. 9.

THEORETICAL PROCEDURE

The life prediction theory used in this study is described in detail in Ref. 1. This theory considers both low-cycle fatigue and cyclic creep (fig. 10). Low-cycle fatigue is assumed to result in failure by transgranular cracking. On the other hand, cyclic creep is assumed to cause intergranular cracking. After a thermal stress analysis, life is calculated separately for each of these two distinct failure modes. A linear interaction between fatigue and cyclic creep is assumed. Thermal fatigue life can then be calculated as follows:

$$\frac{1}{N_t} = \frac{1}{N_c} + \frac{1}{N_f} \tag{1a}$$

or

$$N_t = (\phi_c + \phi_f)^{-1} \tag{1b}$$

in which

N = cycles to failure

ϕ = damage per cycle, 1/N

t, c, f = thermal fatigue, cyclic creep, and low cycle fatigue respectively

Cyclic Creep Theory

Cyclic creep damage, ϕ_c, is calculated from static creep-rupture data. A modification of the life-fraction rules proposed by Robinson and Taira is used (refs. 9 to 11), as follows:

$$\phi_c = \int_0^{\Delta t} \frac{1}{t_r} \, dt \tag{2}$$

in which

t = elapsed time, hr

Δt = time per cycle, hr

t_r = cyclic time to rupture, hr

The cyclic rupture time t_r is a function not only of stress and temperature but also of other factors. A simplified definition of this function is as follows:

$$t_r = k t_{r,s}(|S|, T) \tag{3}$$

in which

$t_{r,s}$ = static creep rupture life, hr

$|S|$ = absolute value of stress during thermal-fatigue cycle, N/cm^2

T = temperature during thermal-fatigue cycle, K

$$k = \begin{cases} 1, \text{ for uncoated alloys} \\ \text{or} \\ \dfrac{D_c(T)}{\epsilon'_c(T)}, \text{ for coated alloys} \end{cases}$$

in which

D_c = average creep ductility at temperature T, %

ϵ_c^* = average "prior creep" (creep during first and second stage) at temperature T, %

The two values of k follow from hypotheses concerning the accumulation of cyclic creep strain. In uncoated alloys, the equivalent of unstable third-stage creep is possible because failure occurs at a free surface. The surface is free to bulge of "neck" locally at grain boundaries or other discontinuities. In this respect, failure is similar to static creep rupture and k is taken equal to 1. On the other hand, an oxidation-resistant coating will support the surface of the substrate. It is assumed that this support prevents instability. Failure then occurs by exhaustion of ductility.

Low-Cycle Fatigue Theory

Fatigue damage ϕ_f is calculated by Manson's Method of Universal Slopes (ref. 12). This is an empirical formula relating mechanical strain range, cycles to failure (or fatigue damage), and conventional tensile properties, as follows:

$$\phi_f = 1/N_f, \text{ fatigue damage}$$

$$\Delta\epsilon_m = 3.5 \frac{UTS}{E} \phi_f^{.12} + 100\, D_t^{.6} \phi_f^{.6} \qquad (4)$$

in which

$\Delta\epsilon_m$ = mechanical strain range, %

UTS = ultimate tensile strength, N/cm^2

E = Young's Modulus, $N/cm^2/\%$

D_t = tensile ductility, cm/cm

Eq. (4) can be solved graphically for ϕ_f using full logarithmic coordinates. The tensile properties are evaluated at the temperature in the cycle which gives the maximum value of ϕ_f (minimum life). This is usually the maximum temperature in the cycle.

Sample Calculations

The first step in life prediction is a thermal stress analysis of the double-wedge specimen. As shown in Fig. 11, data from five thermocouples are fitted by a parabolic curve. This is assumed to be the average chordwise distribution of temperature at a given instant of time. By assuming complete elasticity and that plane cross-sections remain plane, a linear distribution is obtained for spanwise elastic total strain. Subtracting free thermal expansion from this total strain at the two edges of the specimen then gives the critical values of mechanical strain.

Fig. 12(a) shows typical elastic strain and temperature cycles for one edge of a specimen. Fig. 12(b) shows the relationship between strain and temperature. As noted on this curve, compressive creep and tensile plastic strain occur during different parts of the cycle, at different temperatures. This can lead to accumulation of strain at grain boundaries, followed by compressive instability and bulging. These bulges can be crack nuclei. Increasing the cycle time tends to increase the tensile strain more than the compressive strain.

Assuming total strain is independent of small local inelastic strains, stresses can now be calculated. The effect of creep on the stress cycle must also be considered. As shown in Fig. 13, stresses often change from their first-cycle values. This is required to equalize tensile and compressive inelastic strain and produce a stable cycle. This phenomenon is often referred to as "shakedown".

A typical distribution of creep damage rate, $1/t_r$, is shown in Fig. 14. Most of the creep damage occurs during heating, while stresses are compressive. The area under this curve is the creep damage per cycle. The fatigue damage is calculated from the Method of Universal Slopes. Finally, thermal-fatigue life is obtained from the sum of the creep and fatigue damages, as shown in the figure.

COMPARISON OF THEORETICAL AND EXPERIMENTAL RESULTS

Table VI is a summary of the life calculations for IN 100 and B 1900, both coated and uncoated. Experimental lives for these alloys are also given. The data for the 1.0 millimeter radius edge have been adjusted to a 0.6 millimeter radius for ease in comparing experiment and theory. The following formula was used to make this adjustment:

$$N_{adjusted} = N_{observed} \times \frac{N_t(0.6 \text{ mm R.})}{N_t(1.0 \text{ mm R.})} \qquad (5)$$

in which N_t is the theoretical thermal fatigue life (eq. 1b).

Figs. 15 and 16 contain comparisons between theoretical and experimental thermal-fatigue resistances. The theoretical curves in these figures are based on theoretical thermal fatigue lives in Table VI for the 0.6 millimeter radius edge.

The experimental data in Figs. 15 and 16 are the observed lives for the 0.6 millimeter radius edge and adjusted lives for the 1.0 millimeter edge. No data are plotted for edges that did not crack. In certain cases, at cycle times of seven and eight minutes, data are plotted only for the first edge to crack. For these cases, cracks in the first edge apparently delayed cracking in the second edge.

As shown in Fig. 15, cyclic creep was the dominant failure mode for IN 100, both coated and uncoated. Only for the four-minute cycle test on the coated alloy was fatigue calculated to be as important as cyclic creep. Agreement between theory and experiment was generally good. The beneficial effect of the coating was somewhat underestimated by the theory.

The theoretical predictions for uncoated B 1900 (fig. 16(a)) indicated that cyclic creep was again the dominant failure mode. However, for coated B 1900 (fig. 16(b)) both fatigue and cyclic creep were important. Correlation between experiment and theory was as good for this alloy as it was for IN 100.

CONCLUSIONS

The objective of this investigation was to measure the relative thermal-fatigue resistance of 15 alloys under conditions representing advanced turbine engines. The primary purpose for obtaining these data was to verify a life-prediction theory for thermal fatigue. The test program was accomplished using the fluidized-bed technique for rapid heating and cooling.

The test conditions in this study may be quite different from actual use conditions. For this reason, the absolute number of cycles to cracking is not considered to be significant. However, the relative resistance to cracking, as reported herein, is significant for the high temperatures which may be present in advanced turbine engines. At lower temperatures, relative cracking resistance may change somewhat, particularly for those alloys which were tested above their present use temperature.

Under identical test conditions, thermal-fatigue lives varied from 13 to 4700 cycles. The longest lives were obtained with materials that had been either directionally solidifed or coated or both: MM 200 DS, IN 100 DS, IN 100 DS (coated), and B 1900 (coated).

Among the 13 uncoated conventionally cast or wrought alloys, TAZ 8A and X 40 showed the highest thermal-fatigue resistances.

The longest and shortest lives, as rated on the six-minute cycle, were obtained with materials which had the same composition but different grain structures: MM 200 and MM 200 DS. Evidently, structure of the alloy is more important than minor variations in composition.

Examination of crack paths and fracture surfaces showed that cracks tend to be intergranular in alloys with low thermal-fatigue resistance. Alloys with high resistance tended to exhibit transgraular cracking. This indicates that a prerequisite for extending thermal-fatigue life is the suppression of intergranular cracking.

In uncoated IN 100 and B 1900, crack growth rates were inversely proportional to the number of cycles required to start the crack. However, coating these two alloys delayed crack initiation, but did not change the crack growth rate.

Some materials suffered considerable weight loss through oxidation. These tests indicated that directionally solidified materials oxidize more rapidly than the same alloy in the conventionally cast form. Although coating of IN 100 DS somewhat reduced its thermal-fatigue resistance, it greatly reduced the amount of weight loss.

Theoretical thermal-fatigue lives for IN 100 and B 1900, coated and uncoated, were in agreement with experimental data. This appears to verify the stress analysis and the life prediction theory used.

REFERENCES

1. D. A. Spera, The Calculation of Elevated-Temperature Cyclic Life Considering Low-Cycle Fatigue and Creep, NASA TN D-5317, 1969.
2. D. A. Spera, in Aerospace Stuctural Materials Conference, NASA SP-227, Nov. 1969, p. 43.
3. E. Glenny, J. E. Northwood, S. W. K. Shaw, and T. A. Taylor, A Technique for Thermal-Shock and Thermal-Fatigue Testing Based on the Use of Fluidized Solids, Inst Metals, 87 (1958-1959) 294.
4. E. Glenny and T. A. Taylor, A Study of the Thermal-Fatigue Behaviour of Metals. Inst Metals, 88 (1959-1960) 449.
5. A. W. Franklin, J. Heslop, and R. A. Smith, Some Metallurgical Factors Influencing the Thermal-Fatigue Resistance of Wrought Nickel- and Chromium-Base High-Temperature Alloys, Inst Metals, 92 (1963-1964) 313.
6. M. A. H. Howes, Heat Checking in Die Casting Dies, Die Casting Eng, 13, (1969) 12.
7. M. A. H. Howes and Z. P. Saperstein, Thermal-Fatigue of Copper-to-Steel Joints, Welding 48, (1969) 543-S.
8. M. A. H. Howes, Thermal Fatigue Data on 15 Nickel- and Cobalt-Base Alloys, IIT Research Inst. Rep. IITRI-B 6078-38, NASA CR-72738, May 1970.
9. E. L. Robinson, Effect of Temperature Variation on the Long-Time Strength of Steels, Trans ASME, 74 (1952) 777.

10. S. Taira, Creep in Structures, ed. N. J. Hoff, Springer-Verlag (Berlin), 1962, p. 96.

11. D. A. Spera, A Linear Creep Damage Theory for Thermal Fatigue of Materials, Ph.D. Thesis, Univ. of Wisconsin, 1968.

12. S. S. Manson, Fatigue: A Complex Subject--Some Simple Approximations, Soc Exper Stress Anal, 5, (1965) 193.

TABLE I. - COMPOSITIONS OF ALL ALLOYS AND COATING USED IN THE EXPERIMENTAL PROGRAM

	Additional specification	Cast number	Composition, wt %												
			C	Mn	Si	Cr	Ni	Co	Mo	W	Al	Ti	Zr	B	Other
Nickel base alloys															
*B 1900		54V6335	0.10	0.10	<0.10	8.11	Bal.	10.15	6.11	< 0.10	6.09	0.98	0.08	0.013	4.28 Ta, 0.16 Fe, 4.28 V
*IN 100		KJ 2206	0.17	<0.02	0.11	10.30	Bal.	15.10	2.96	---	5.45	4.76	0.084	0.016	0.21 Fe, 0.97 V
*IN 100 DS	PWA 1401	KJ 2206	0.17	<0.02	0.11	10.30	Bal.	15.10	2.96	---	5.45	4.76	0.084	0.016	0.21 Fe, 0.97 V
MM 200		KD 2012	0.15	<0.02	0.080	9.20	Bal.	10.25	---	12.55	5.05	2.13	0.048	0.017	0.36 Fe, 0.96 Cb, <0.01 V
MM 200 DS	PWA 664	KD 2012	0.15	<0.02	0.080	9.20	Bal.	10.25	---	12.55	5.05	2.13	0.048	0.017	0.36 Fe, 0.96 Cb, <0.01 V
IN 162		96317	0.10	0.01	0.04	10.03	Bal.	0.03	4.05	2.03	6.35	0.93	0.11	0.018	1.97 Ta, 0.17 Fe, 0.88 Cb
IN 713 C		65611	0.11	<0.10	<0.10	13.40	Bal.	---	4.50	---	5.95	0.83	0.08	0.009	2.24 Cb + Ta, 0.27 Fe
M 22		67-635	0.06	---	---	6.35	Bal.	---	1.96	11.37	6.24	---	0.65	---	2.87 Ta
TAZ 8A		67-640	0.01	---	---	6.20	Bal.	---	3.86	3.86	5.96	---	0.88	---	8.01 Ta, 2.44 Cb
U 700, cast		85V2416	0.08	<0.10	<0.10	14.24	Bal.	14.87	4.18	---	4.25	3.26	<0.01	0.012	0.30 Fe
U 700, wrought		6541	0.113	0.01	0.02	14.85	Bal.	17.50	5.10	---	4.55	3.45	<0.02	0.013	0.85 Fe
**TD NiCr		1862	0.038	---	---	21.39	Bal.	---	---	---	---	---	---	---	2.5 Th O_2, 0.0005 N, 0.006 S
		2858	0.020	---	---	19.72	Bal.	---	---	---	---	---	---	---	1.9 Th O_2, 0.004 N, 0.007 S
Cobalt base alloys															
X 40		12C6412	0.48	<0.05	0.33	25.59	10.52	Bal.	0.04	7.87	---	---	0.03	0.005	0.46 Fe, 0.02 N
WI 52		59-682	0.46	0.21	0.28	20.86	0.23	Bal.	<0.05	11.06	---	---	---	---	1.75 Fe, 1.87 Cb
MM 302		T 272	0.88	<0.10	0.22	21.9	0.49	Bal.	<0.1	9.89	---	---	0.24	<0.01	8.80 Ta, 1.11 Fe
Coating															
Jocoat	PWA 47		Nominal composition 10.0 Si, 90.0 Al												

*Tested coated and uncoated.

**Relatively large thickness of 0.62 cm prevented adequate dispersion of Thoria (ref. 8).

TABLE II. - HEAT TREATMENTS FOR SPECIMENS

Alloy	Solution treatment		Intermediate aging		Final aging	
	Temp. K	Time hrs.	Temp. K	Time hrs.	Temp. K	Time hrs.
B 1900	----	----	----	----	1116	24
IN 100	1422	2	----	----	1200	16
IN 100 DS	1422	2	----	----	1200	16
MM 200	----	----	----	----	1089	50
MM 200 DS	----	----	----	----	1089	50
U 700, cast	----	----	----	----	1033	16
U 700, wrought	1394	4	1116	24	1033	16
X 40	----	----	----	----	1033	50
MM 302	1505	8	----	----	1089	24

All other materials were used in the as-cast condition.

TABLE III. - TENSILE PROPERTIES AT 1030 K (1400 F)

Alloy (none coated)	Proportional limit		Ultimate Tensile Strength		Reduction of Area, %
	N/cm^2	% of Nominal 0.2% YS	N/cm^2	% of Nominal UTS	
B 1900	93,800	116	109,000	114	8
IN 100	79,300	92	96,500	90	13
IN 100 DS	84,100	---	103,400	107	16
MM 200	85,500	102	100,000	107	5
MM 200 DS	No specimens available.				
IN 162	89,600	106	112,400	112	11
IN-713C	81,400	109	101,400	108	12
M22	95,800	124	105,500	116	8
TAZ 8A	103,400	---	120,000	134	2
U 700 (cast)	74,500	98	102,000	114	16
U 700 (wrought)	75,800	92	98,600	95	30
TD NiCr	29,000	105	32,400	107	6
X 40	38,600	125	59,300	123	20
WI 52	57,900	168	76,500	126	7
MM 302	69,600	180	80,000	115	3

Each result is the average of two tests.

TABLE IV. - CREEP-RUPTURE PROPERTIES AT 1255 K (1800 F)

Alloy (none coated)	Stress	Life (nominal 100 hour)			Reduction of Area %
	N/cm^2	hours		% of Nominal	
B 1900	17,200	99,	95	97	11
IN 100	17,200	94,	70	82	16
IN 100 DS	15,900	144,	164	154	62
MM 200	17,900	114,	73	94	10
MM 200 DS	no specimens available				
IN 162	16,500	115,	71	93	10
*IN 713C	14,500	75,	54	64	22
*M22	20,000	7.5,	11	9 [illegible]	4
TAZ 8A	12,400	89,	79	84	8
U 700 (cast)	12,400	121,	118	120	22
U 700 (wrought)	11,000	141,	133	137	32
*TD NiCr	7,600	0.1,	---	0.1	3
**TD NiCr	3,400	1268,	---	NA	6
X 40	7,600	183,	>105	183	33
WI 52	9,000	158,	153	156	15
MM 302	9,700	69,	95	82	8

* Rupture strength significantly lower than published data.

** Supplementary test.

TABLE V. - THERMAL CYCLES REQUIRED TO CAUSE CRACKING (BED TEMPS: 1360 K AND 590 K)

Time per cycle, min.		4	4	5	6	7	8	Percent of TAZ 8A life	
Temp., 0.6 mm radius, K	max.	1295	1295	1315	1330	1335	1340		
	min.	670	670	640	625	610	605	6 min. cycle	All cycles
Alloy		Cycles to first crack[a]							
MM 200 DS		>5000	>5000	>2000	4700	>1400	>1500	800	>300
IN 100 DS		>5000	>5000	>2000	4200	>1400	>1500	700	>300
IN 100 DS, coated		900	1700	>2000	2400	>1400	>1500	400	>200
B 1900, coated		1700	3500	1200	1190	>1400	850	200	>100
TAZ 8A		3500	2500	850	600	1200	850	100	100
X 40		713	713	600	600	600	400	100	50
IN 100, coated		1700	>1000	1200	400[b]	250	400[b]	70	> 60
B 1900		900	713	400	400	600	400	70	40
IN 162		1700	713	400	400	400	250	70	40
IN 713C		900	900	400	250	600	250	40	40
TD NiCr		1000[c]	1000[c]	400	250	75	75	40	30
MM 302		900	713	250	75	400	400	10	30
WI 52		900	537	250	75	250	150	10	20
U 700, cast		900	166	150	75	250	150	10	20
IN 100		900	537	75	38	75[b]	38	6	10
M 22		375[b]	375[b]	13	13	13[b]	250	2	10
U 700, wrought		166	166	75	13	38	13	2	5
MM 200		166	166	38	13	13	13	2	4

[a]cracks in edge with 0.6 mm radius, unless noted otherwise.

[b]crack in edge with 1.0 mm radius.

[c]longitudinal cracks from ends.

TABLE VI. - THEORETICAL AND EXPERIMENTAL THERMAL FATIGUE LIVES

Edge radius, mm	Cycle time, mm	Strain range, %	Max. temp., K	Uncoated					Coated				
				Theoretical life, cycles			Experimental life, cycles		Theoretical life, cycles			Experimental life, cycles	
				Fatigue, N_f	Cyclic creep, N_c	Thermal fatigue, N_t	Observed, N_{obs}	Adjusted to 0.6 mm R., N_{adj}	Fatigue, N_f	Cyclic creep, N_c	Thermal fatigue, N_t	Observed, N_{obs}	Adjusted to 0.6 mm R., N_{adj}
IN 100 Alloy													
0.6	4	0.65	1311	3000	570	480	537, 900	same	3000	3100	1500	1700, >1000	same
	5						75					1200	
	6	0.75	1339	1700	55	53	38		1700	270	230	600	
	7						250					250	
	8	0.80	1344	1400	37	36	38		1400	180	178	1250	
1.0	4	0.58	1300	5000	2100	1480	713, >1000	230, >320	5000	10,400	3400	3500, >1000	1550, >440
	5						400	160				1200	560
	6	0.67	1339	2400	113	108	150	74	2400	570	460	400	200
	7						75	56				>1400	>1050
	8	0.72	1344	1900	40	39	400	370	1900	200	180	400	395
B 1900 Alloy													
0.6	4	0.68	1238	3000	2380	1330	713, 900	same	3000	8400	2210	1700, 3500	same
	5						400					1200	
	6	0.73	1327	1800	720	520	400		1800	2520	1050	1190	
	7						600					>1400	
	8	0.74	1344	1600	410	330	400		1600	1420	750	850	
1.0	4	0.60	1272	5500	10,700	3620	3500, >1000	1290, >370	5500	36,400	4800	3500, 4500	1600, 2100
	5						1200	500				>2000	>1040
	6	0.65	1316	2500	2000	1110	800	380	2500	6870	1830	1700	980
	7						600	280				>1400	>780
	8	0.66	1344	2200	1120	740	400	180	2200	3800	1390	>1500	>810

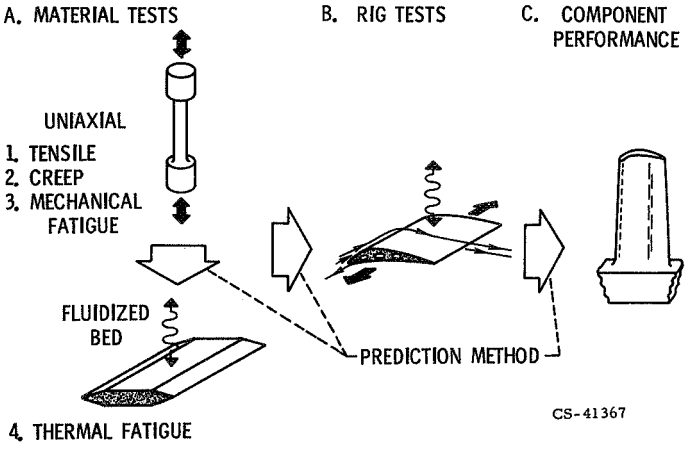

Figure 1. - Thermal fatigue program.

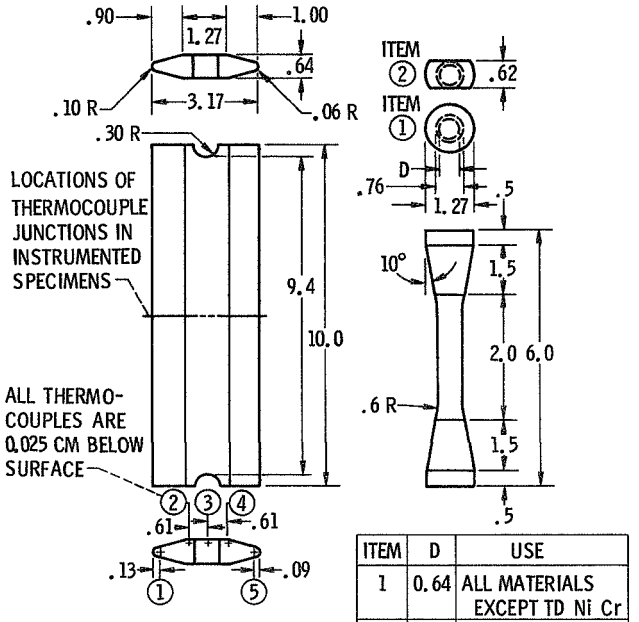

ITEM	D	USE
1	0.64	ALL MATERIALS EXCEPT TD Ni Cr
2	.50	TD NiCr ONLY

(A) THERMAL FATIGUE TEST SPECIMEN. (B) UNIAXIAL TEST SPECIMEN.

Figure 2. - Test specimens (all dimensions in cm.).

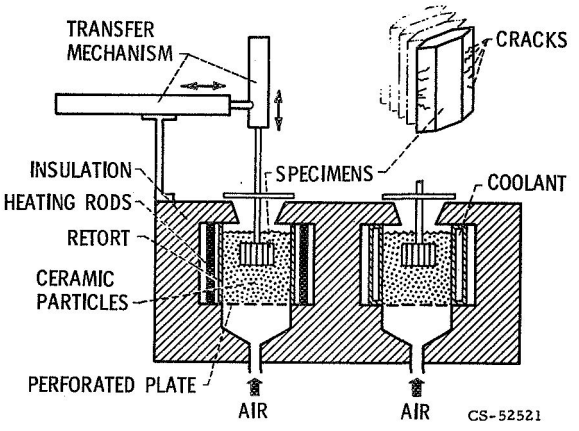

Figure 3. - Fluidized-bed thermal fatigue facility.

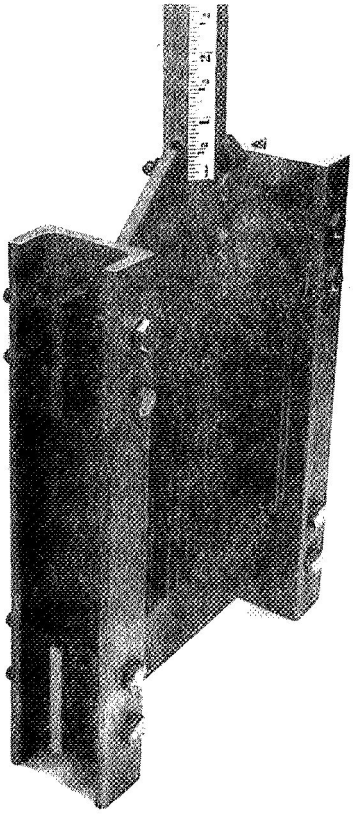

Figure 4. - Holding fixture with group of 18 specimens (scale in inches: 1 in. = 2.54 cm).

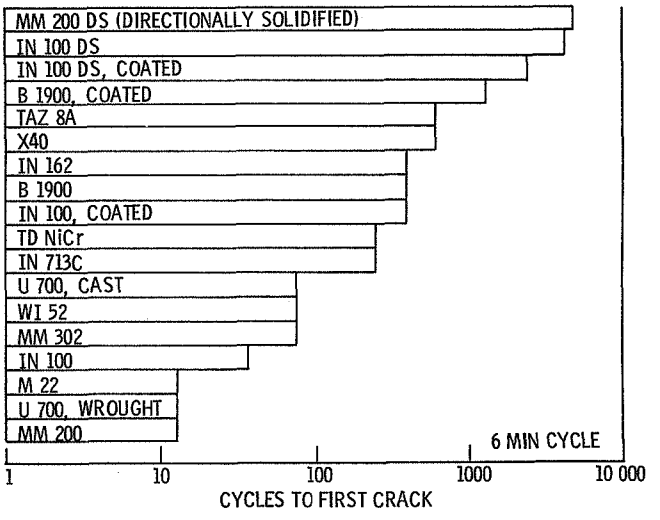

Figure 5. - Comparative thermal fatigue resistance for fluidized-bed tests. (Bed temperatures 590 K ⇌ 1360 K).

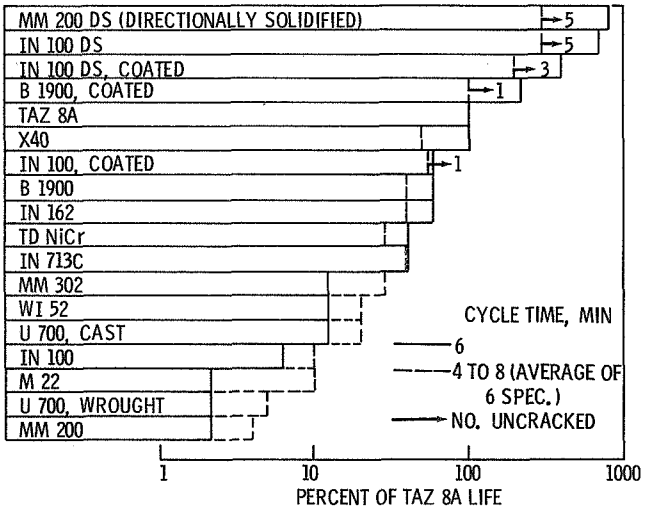

Figure 6. - Relative thermal fatigue resistance for fluidized-bed tests. (Bed temperatures 590 K ⇌ 1360 K).

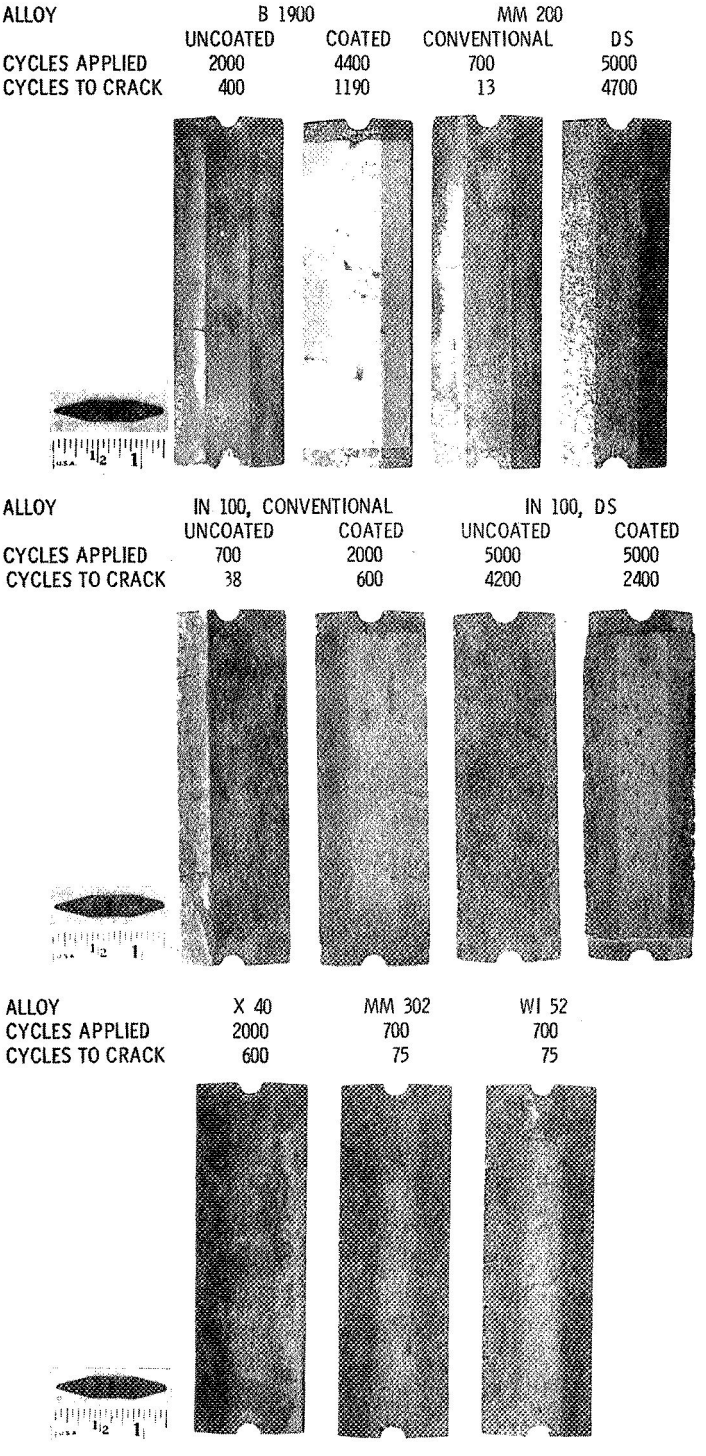

Figure 7. - Thermal-fatigue specimens after testing. (Scale in inches: 1 in. = 2.54 cm. Bed temperatures: 590 K ⇌ 1360 K per 6 min. cycle.)

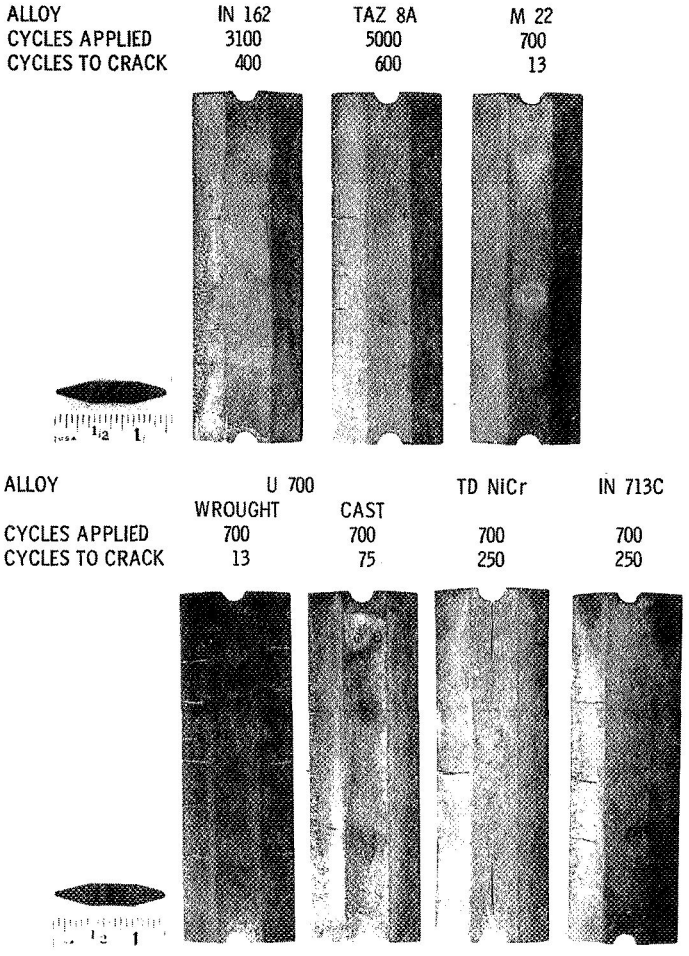

Figure 7. - Concluded.

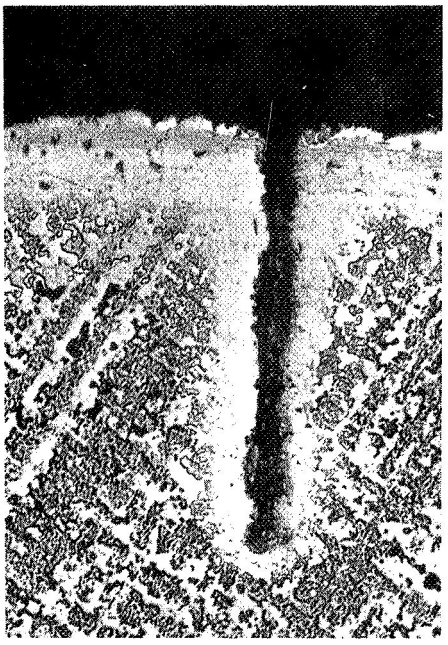

TAZ 8A

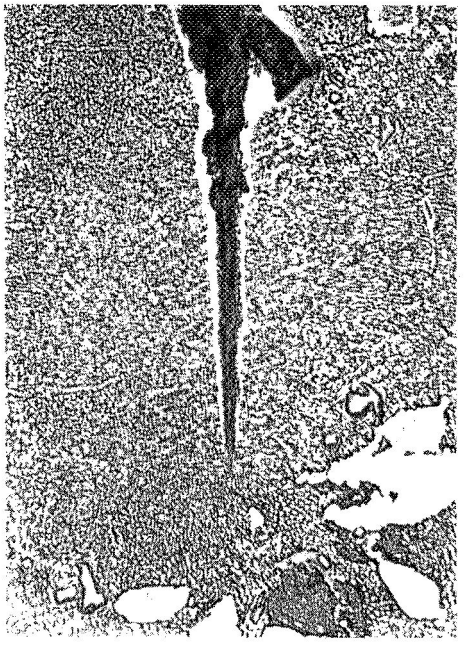

IN 100 DS

(a) Transgranular. Tested for 5000 6-minute cycles.

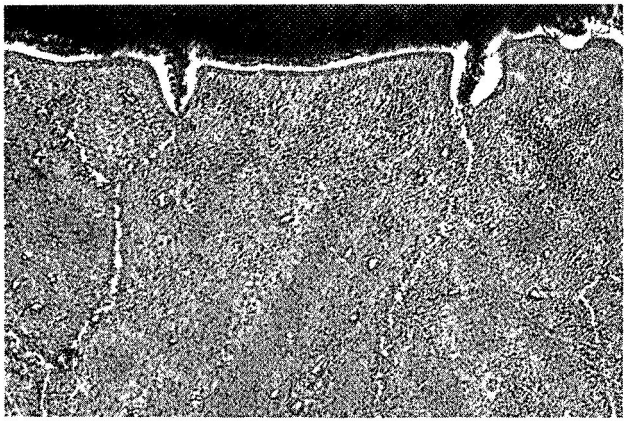

MM 200

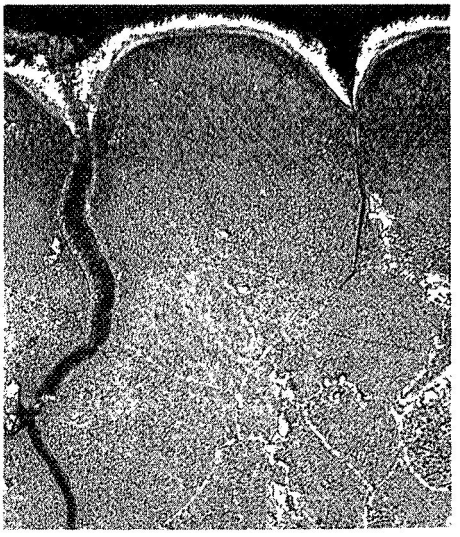

U 700, WROUGHT

(b) Intergranular. Tested for 700 6-minute cycles.

Figure 8. - Thermal fatigue cracks. Bed temperatures: 590 K⇌1360 K per 6-minute cycle. X500.

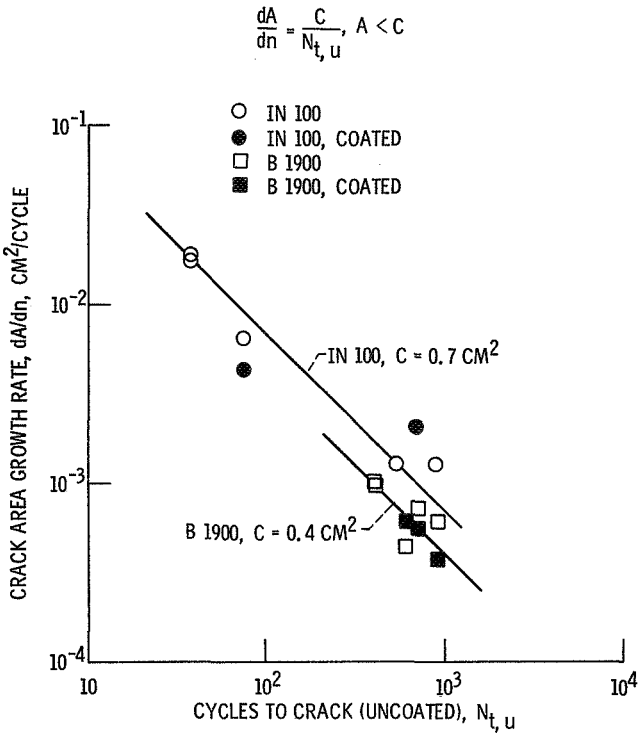

Figure 9. - Crack area growth rate as a function of cycles to first crack for IN 100 and B 1900.

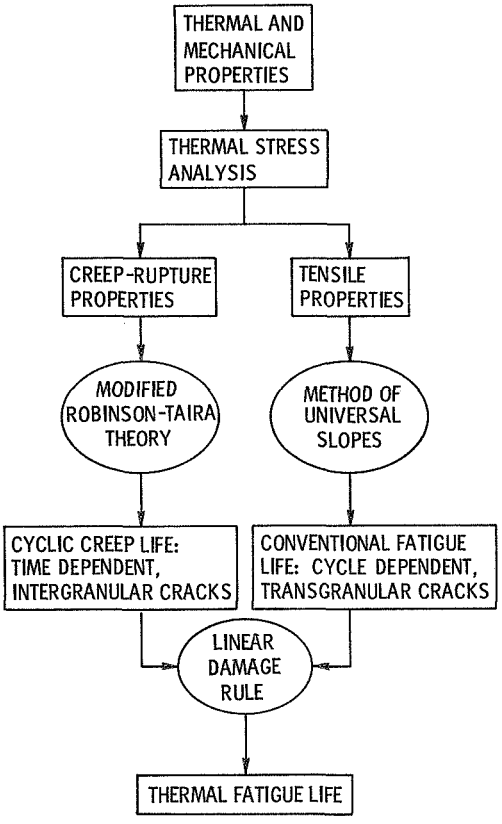

Figure 10. - Schematic representation of life prediction method.

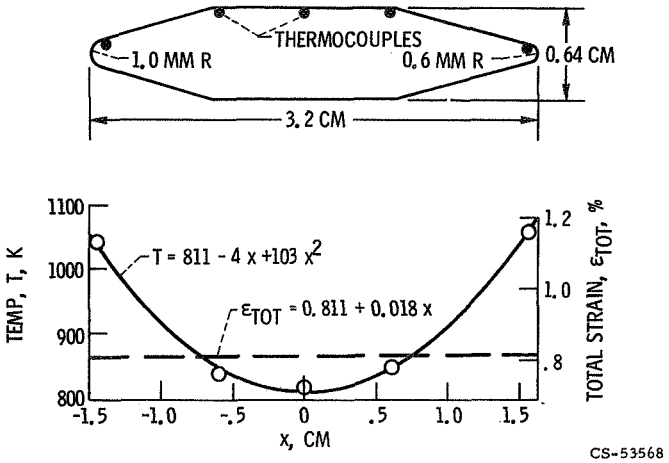

Figure 11. - Typical temperature and total strain distributions. (IN 100 alloy after 12 sec heating.)

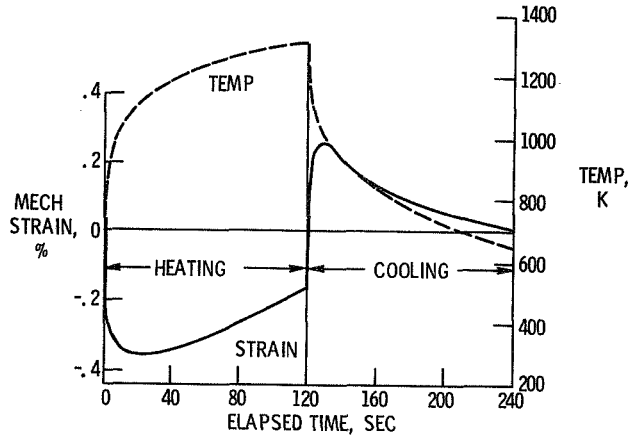

(A) STRAIN AND TEMPERATURE VERSUS TIME.

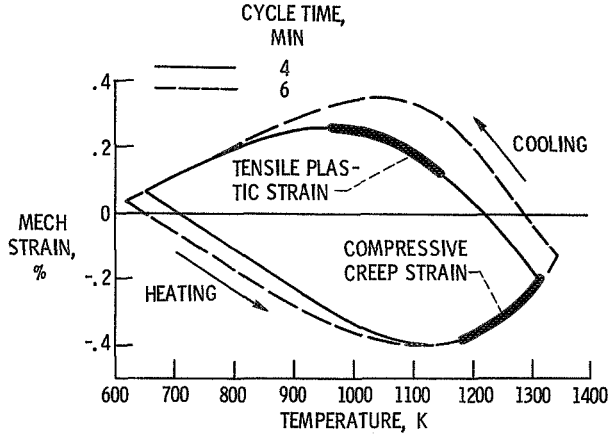

(B) STRAIN VERSUS TEMPERATURE.

Figure 12. - Typical strain and temperature cycles. (IN 100 alloy at 0.6 mm radius edge).

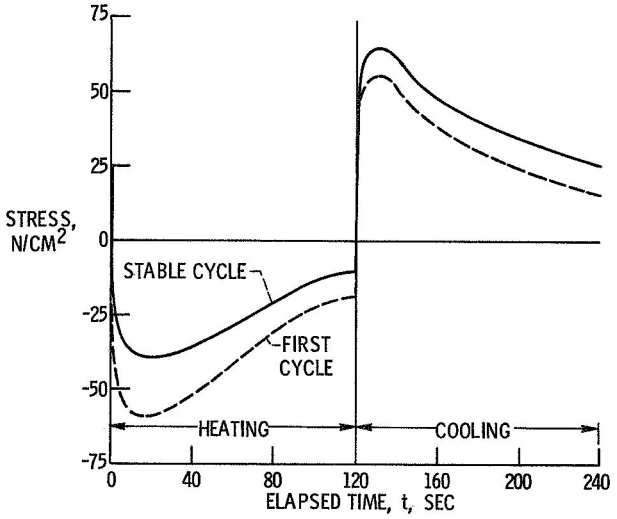

Figure 13. - Typical stress cycles. (IN 100 alloy at 0.6 mm radius edge.)

FATIGUE LIFE = 3000 CYCLES (BY UNIVERSAL SLOPES)
FATIGUE DAMAGE = 1/3000 = 0.00033/CYCLE
CREEP DAMAGE = 0.00175/CYCLE
TOTAL DAMAGE = 0.00175 + 0.00033 = 0.00208/CYCLE
THERMAL FATIGUE LIFE = 1/0.00208 = 480 CYCLES

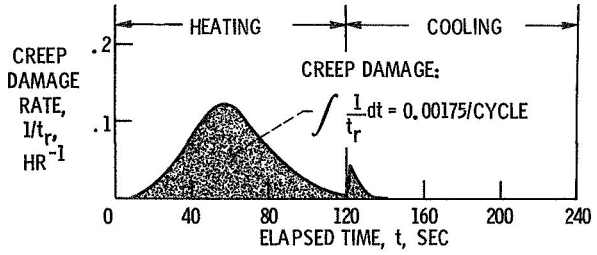

Figure 14. - Typical creep damage and calculation of thermal fatigue life. (IN 100 alloy, bed temperatures 590 K⇌1360 K).

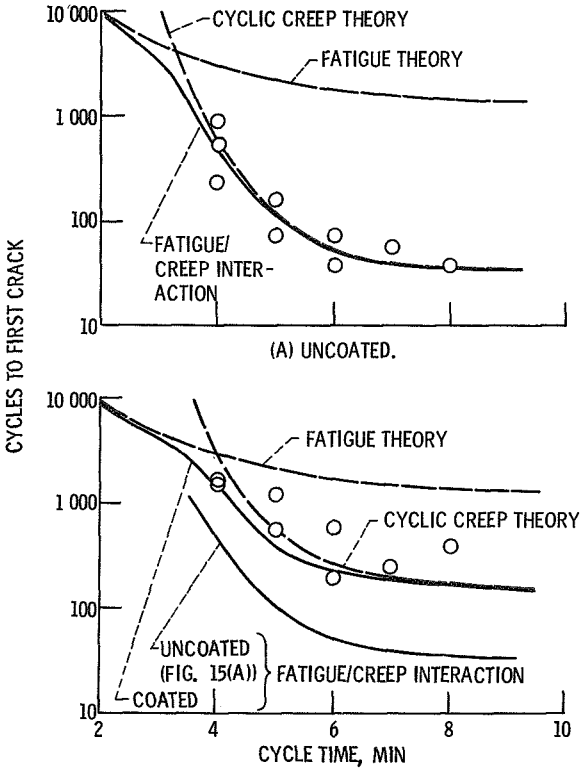

Figure 15. - Comparison of experimental and theoretical thermal fatigue resistance of IN 100 alloy. (Bed temperatures 590 K⇄1360 K.)

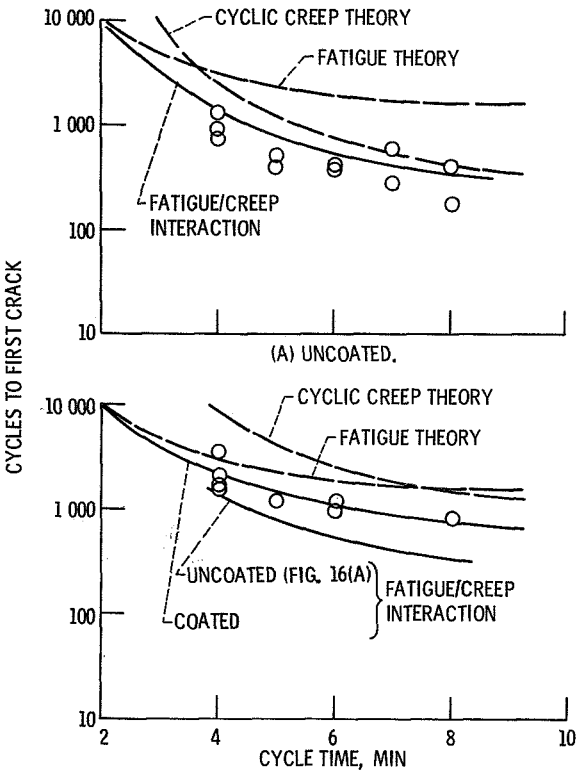

Figure 16. - Comparison of experimental and theoretical thermal fatigue resistance of B 1900 alloy. (Bed temperatures 590 K⇄1360 K).